


PSFC/JA-00-19

**Impurity Transport Experiments in the Edge Plasma of
Alcator C-Mod using Gas Injection Plumes**

View metadata, citation and similar papers at core.ac.uk

brought to you by  C
provided by DSpace

July 2000

Plasma Science and Fusion Center
Massachusetts Institute of Technology
Cambridge, MA 02139 USA

¹Acadia University, Dept. of Pure and Applied Science, Wolfville, Nova Scotia, Canada B0P 1X0

This work was supported by the U.S. Department of Energy, Cooperative Grant No. DE-FC02-99ER54512. Reproduction, translation, publication, use and disposal, in whole or in part, by or for the United States government is permitted.

Submitted for publication to *Journal of Nuclear Materials*.

Impurity Transport Experiments in the Edge Plasma of Alcator C-Mod using Gas Injection Plumes

S. Gangadhara ^a, B. LaBombard ^a

^a*M.I.T. Plasma Science and Fusion Center, 175 Albany St., Cambridge, MA
02139 USA*

C. MacLatchy ^b

^b*Acadia University Dept. of Pure and Applied Science, Wolfville, Nova Scotia,
Canada B0P 1X0*

Abstract

Understanding impurity and bulk plasma transport in the scrape-off layer (SOL) of tokamak plasmas is critical for the design of future reactors. The development of a system on Alcator C-Mod for inferring impurity transport behaviour parallel and perpendicular to local magnetic field lines from impurity emission patterns (“plumes”) generated by local gas injection will be presented. Gas is injected at variable location in the SOL through the end of a reciprocating fast-scanning probe. Carbon plumes are generated by puffing ethylene gas (C₂H₄) through the probe over a period of ~ 8-10 ms. Two intensified CCD cameras are used to record C⁺¹ and C⁺² emission patterns from near-perpendicular views. Flows parallel and perpendicular to the magnetic field have been observed in both views. In principle, the data allow a full 3-D reconstruction of the impurity dispersal with ~ 1 mm spatial resolution.

Key words: Alcator C-Mod; Impurity transport; Plumes.

1 Introduction

The transport of impurities along and across field lines in the edge plasma is of fundamental importance to reactor operation. High impurity concentrations in the core can lead to degradation of core energy confinement, whereas high edge concentrations can lead to significant radiation of power entering the scrape-off layer (SOL) and a re-distribution of this power over a large surface area.

A direct means of inferring information about impurity transport in the edge plasma is to inject impurities locally into the SOL and study the resultant impurity dispersal patterns (“plumes”). Such studies have been previously conducted on Alcator C-Mod [1], but were limited to injection of gas through wall capillaries. This limited the type of plasmas studied to those in the far SOL, near the wall. In addition, impurity line emission was viewed with a single camera system, providing no information about the transport of impurities across flux surfaces.

A novel new design for a reciprocating fast-scanning probe was developed during the 1997 Alcator C-Mod run campaign, allowing for injection of gas through the probe tip [2]. With this design, impurity atoms can be injected locally at variable position in the SOL, including deep into the SOL, up to the last closed flux surface (LCFS). Transport studies can be conducted as a function of SOL position. An additional advantage is that the local plasma density and temperature are measured *directly* at the injection location via the probe. These data can be used in modeling the resulting impurity emission plumes, imaged from two near-perpendicular camera views.

In this paper, we report initial results and progress towards developing a system to infer impurity transport from the dispersal of C^{+1} and C^{+2} plumes.

2 Experimental Arrangement

2.1 Fast-Scanning Probe

A cross-section of the Alcator C-Mod vacuum chamber with a layout of the main diagnostics for the gas-injection system is shown in Figure 1. A reciprocating fast-scanning probe (FSP), containing four Langmuir probe elements, is used to obtain cross-field profiles of electron density and temperature in the SOL. Probe pairs are oriented along and across the local magnetic field, yielding estimates of the parallel and cross-field flow profiles in the SOL.

A detailed diagram of the FSP head is shown in Figure 2. A 1 mm diameter capillary tube located between the probe elements extends down the body of the probe, and is connected to a nearby gas plenum. At the tip of the capillary, inside the probe head, a small inertial gas valve has been inserted. This valve is designed to open when the de-acceleration force on the probe head exceeds $\simeq 30$ g’s, corresponding to a ~ 10 ms time window at the probe end-of-stroke. Thus, gas is injected on flux surfaces within $\simeq 5$ mm of the location of deepest

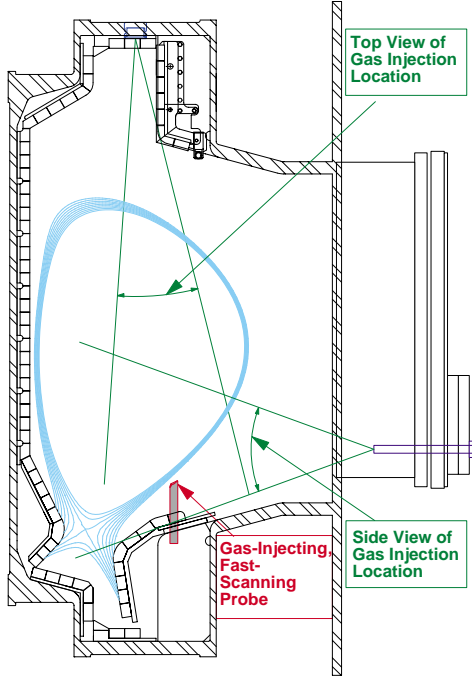


Fig. 1. Cross-section of the Alcator C-Mod vacuum chamber with a typical diverted equilibrium. Gas is injected at the end of stroke of a vertically-scanning probe. Impurity emission plumes are viewed from two near-perpendicular locations.

probe insertion.

2.2 Views Of Emission

Two near-perpendicular views of the scanning probe are available on Alcator C-Mod, and are shown in Figure 1. Plume emission at each location is viewed with a fiber optic bundle containing a square array of 400x400 individual fibers spaced 10μ apart. A camera lens is attached to each bundle, and the bundle is placed (approximately) at the focal plane of the lens. This sets the field of view for each system: for the side view it is $\simeq 27 \text{ cm} \times 27 \text{ cm}$ and for the top view it is $\simeq 23 \text{ cm} \times 23 \text{ cm}$. The viewing resolution of each system is $\simeq 0.6 \text{ mm/fiber}$.

The fiber bundles are optically coupled to gated, intensified CCD cameras [3] through another set of camera lenses. Bandpass interference filters are used to view emission from C^{+1} and C^{+2} . Filters are placed in a filter wheel assembly located between the fiber and the camera, allowing different filters to be selected for different discharges.

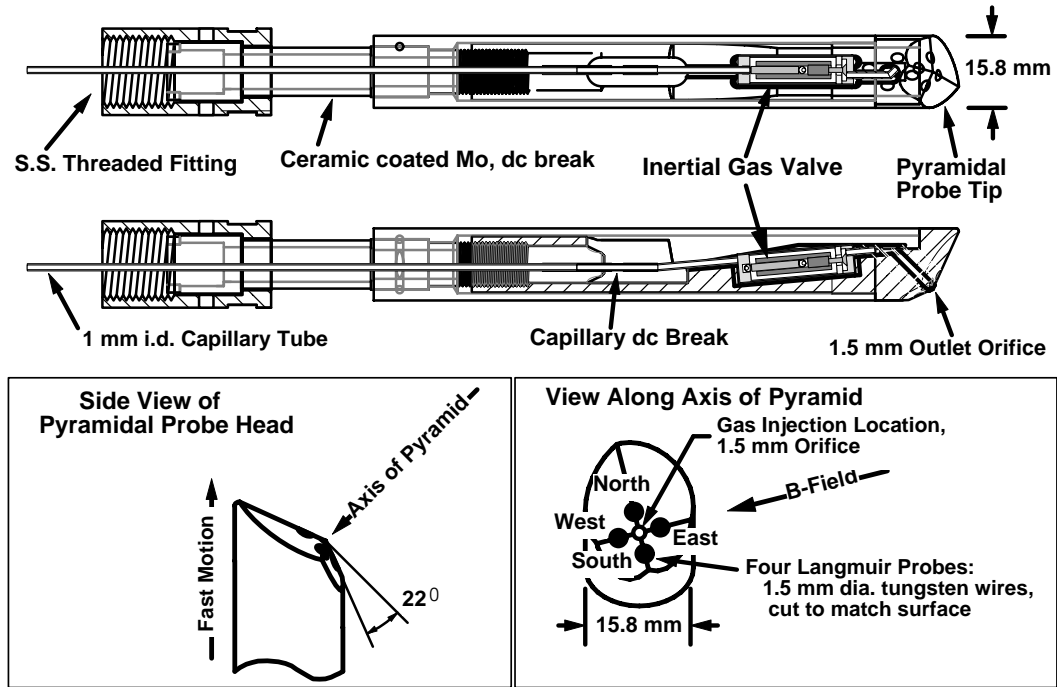


Fig. 2. (Top) Transparent view of fast-scanning probe head assembly showing gas feed and inertial valve location. (Bottom) Close-up views of pyramidal probe tip (actual scale). The materials are: molybdenum ~ body of the probe head, stainless steel ~ capillary tubes and inertial valve, tungsten ~ Langmuir probes, alumina and alumina coating ~ electrical insulation.

2.3 Typical Set-Up Conditions

For these experiments ethylene (C_2H_4) was used as the working gas. For a typical carbon plume, a plenum pressure of $\simeq 16$ - 17 torr is used, resulting in $\sim 5 \times 10^{16}$ molecules of ethylene injected per probe scan. Previous tests indicate that the injection duration is $\simeq 8$ - 10 ms [2], corresponding to the probe de-acceleration time. Assuming *complete* dissociation of the molecule and *complete* ionization of each atom, each probe puff would contribute $\sim 8 \times 10^{17}$ electrons, or less than one percent of the electron inventory in the plasma.

The local perturbation of the plumes can be assessed by a particle and power balance over the region where the impurities enter the plasma. Impurities enter both by direct ionization of injected molecules and via recycling off of the probe head. Results from section 5.2 indicate that the carbon neutral profile width is \sim the probe diameter (see Fig. 5, CII case), implying that the ionization volume is \sim a few cm^3 . Assuming that ions formed in this volume leave along field lines at \sim the sound speed, an estimate for the local impurity

ion density is $\sim \frac{10^{18}}{\sqrt{T_{e,eV}}} \text{ m}^{-3}$. Based on these estimates, the local perturbation of the plumes is small.

For gas-injection levels described above, camera exposures are set between $\sim 50\text{-}100 \mu\text{s}$, depending on the camera and the specific discharge in which the plume is forming. For times this short, the motion of the probe is “frozen”, and the cameras are effectively taking a snap-shot of the emission pattern resulting from a steady flow of injected gas.

3 General Observations for C_2H_4 Plumes

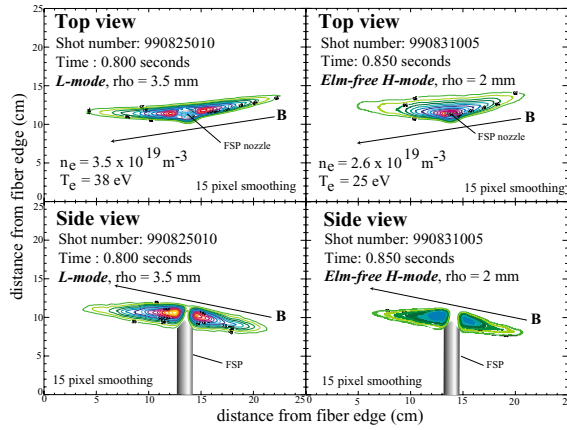


Fig. 3. Smoothed CIII (465.3 nm) emission data from the top and side views. Data on the left was taken during Ohmic L-mode, and data on the right during Ohmic H-mode. A schematic of the probe head is drawn in each figure to indicate its perturbation. An approximate local magnetic field direction is indicated to orient the emission.

False color images of CIII (465.3 nm) emission recorded by the CCD cameras are shown in Figure 3 for an ohmic L-mode and an ohmic H-mode discharge. In the side view, emission is partly obscured by the probe head, while in the top view the probe head contributes some reflected light. A schematic of the probe head is shown in each figure. Emission is extended in the direction along the local magnetic field line. The extent of the emission parallel to \mathbf{B} varies with discharge conditions, and is generally consistent with calculations of the ionization mean-free path made using local density and temperature measurements from the scanning probe. Typical parallel extents for CII (C^{+1}) emission are $\sim 5\text{-}10$ cm, while for CIII (C^{+2}) emission they are $\sim 15\text{-}20$ cm.

Asymmetries are seen in the parallel extent of the CIII emission relative to the injection location. The direction of the asymmetry indicates a flow direction

for the impurity ions. However, for $T_e \geq 35$ eV, the average lifetime of C^{+2} ions is shorter than the average parallel momentum transfer time between C^{+2} and D^+ . Parallel impurity flows are therefore not representative of bulk plasma flow for these cases, or in general for conditions deep in the SOL, where temperatures are high.

Asymmetries are also seen in the cross-field direction of the emission. Figure 3 (side views) shows that the tails of the emission are bent further off of the axis of emission as distance is increased from the injection location. This “boomerang” effect is due to the $\mathbf{E} \times \mathbf{B}$ drift of impurity ions. For the majority of plumes studied, this effect is in a direction implying an E_r that is directed radially *outward*, even up to the LCFS.

Figure 3 shows that discharge conditions affect the emission patterns. During L-mode discharges, emission tends to be very elongated along field lines with little cross-field spreading, whereas in H-mode emission is much more cross-field spread, possibly due to strong $\mathbf{E} \times \mathbf{B}$ flows. Emission patterns can also vary depending on the character of the H-mode (Elm-free vs. EDA), which may be related to changing electric field structure or changing particle transport [4].

4 Emission Alignment and Calibration

For a more quantitative analysis of the plume data, alignment and calibration is necessary. To align the emission to an absolute coordinate space, the vacuum vessel was back-illuminated with a light source, providing images of the machine from both views. Using known coordinates of machine components in the field of view, such as bolts, tiles, etc., a virtual vacuum vessel was numerically generated with geometrical optics, and then aligned to the actual views of the vessel. Impurity emission is aligned using the same transformations that were used to align the virtual vacuum vessel.

Images captured by the video frame-grabber board are digitized, and emission is recorded as a byte value ranging from 0 to 255. To calibrate each system, a light source of constant, known brightness was placed in front of the fiber bundle of each system. Calibrations were obtained for views through both CII (514.1 nm) and CIII (465.3 nm) filters.

Examples of calibrated and aligned CII and CIII plume data are shown in Figure 4. Typical plume brightnesses are in the range of 0.1-1 kW/m²/ster. Using the known coordinates of the emission and the EFIT magnetic recon-

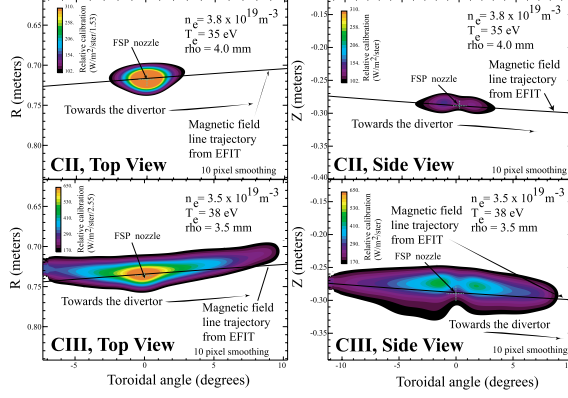


Fig. 4. Aligned and calibrated CII (514.1 nm) and CIII (465.3 nm) emission data, top and side views. Data is taken from Ohmic L-mode discharges (CII: discharge 990825011, CIII: discharge 990825010) at 0.80 seconds. Magnetic field line trajectories obtained from EFIT are overlotted.

struction code [5], the magnetic field line trajectory at the injection location can be overlaid on top of the plumes. This has been done in Figure 4. It is observed that the emission is indeed extended *along* the magnetic field line as expected, but that there can be significant deviation of emission from the field line, indicative of strong cross-field transport. The radial and vertical extents of the emission are comparable for the CIII case, and are ~ 5 cm.

5 Initial Results

5.1 $\mathbf{E} \times \mathbf{B}$ flow estimates

Estimates of the local $\mathbf{E} \times \mathbf{B}$ flow velocity can be obtained by measuring the deviation of C^{+2} plume emission from the local magnetic field line, assuming the dominant drift is due to $\mathbf{E} \times \mathbf{B}$ motion. If the full extent of the plume along \mathbf{B} is seen by the cameras, then $v_{\mathbf{E} \times \mathbf{B}} \simeq d/\tau$, where d is the distance that the tip of the plume has deviated from the field line, and τ is the ionization lifetime of C^{+2} estimated using local electron density and temperature measurements.

For the case shown in Figure 4, $d \simeq 1.5$ cm (averaging top and side view data) and $\tau \simeq 9.3 \mu\text{s}$. This results in $v_{\mathbf{E} \times \mathbf{B}} \simeq 1.6 \times 10^5$ cm/s, or 1.6 km/s. For $|\mathbf{B}| \simeq B_\phi = 4.86$ T, a radial electric field of $E_r \simeq 7.3$ kV/m would be inferred. Floating potential and temperature data obtained from the scanning probe for this discharge at the time of plume formation indicate a radial electric field of 7.6 kV/m, consistent with this estimate.

5.2 1-D Normalized Brightness Profiles

Integration of plume emission data along and across local magnetic field lines can be performed using known emission and field line coordinates. Normalized 1-D profiles of CII and CIII emission across \mathbf{B} obtained from integration of data shown in Figure 4 are shown in Figure 5. In principle, profile asymmetries can be related to impurity flows, while differences in CII and CIII profile widths can be used to determine cross-field diffusivities.

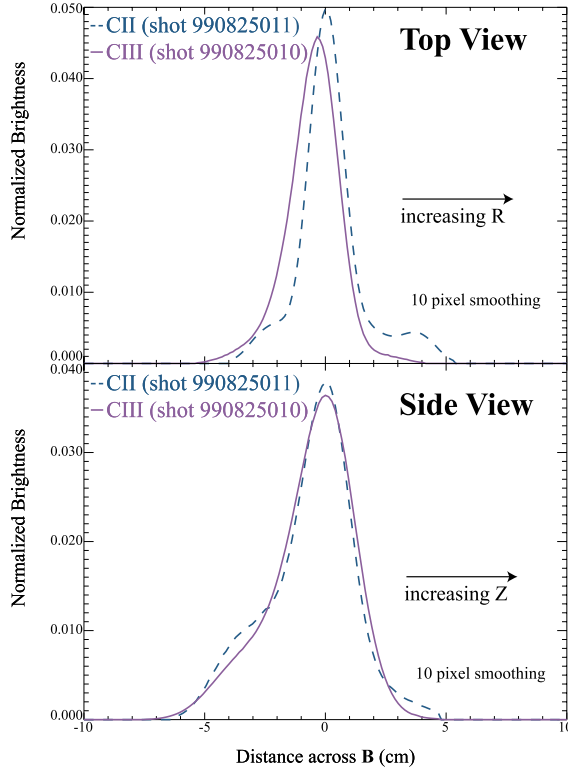


Fig. 5. 1-D profiles of CII (dashed) and CIII across \mathbf{B} , top and side views. These profiles result from the integration of data shown in Fig. 4. Profiles are normalized such that the integral under the curve is unity for all cases. Directions of increasing R and Z are indicated.

Geometry plays an important role in understanding results from both views. In these 1-D profiles, poloidal and radial components of the transport have not been unfolded. Thus, asymmetries in the profiles implying radially (top view) or vertically (side view) directed flows could simply be the result of large $\mathbf{E} \times \mathbf{B}$ flows *along* the flux surface dominating the picture. To determine these flows accurately, a full 3-D model of the plume emission is required.

Differences between CII and CIII profile widths are small, of order 20 percent of the widths themselves. This implies a large neutral (CI) profile width

(relative to the probe injection diameter) arising from specifics of molecular break-up and ion formation. Any estimate of D_{\perp} inferred from these profile differences will be very sensitive to errors in the profile measurements. The validity of comparing CII and CIII data from different discharges, where gas levels, injection location, and background plasma parameters may vary, is therefore questionable. An accurate profile comparison *is* possible for CII and CIII data collected from the *same* plume. Beam-splitter optics have therefore been designed and are being installed to allow each camera to view C^{+1} and C^{+2} emission *simultaneously* for any discharge.

6 Summary and Future Plans

A novel system for determining impurity transport in the SOL is operational on Alcator C-Mod. A reciprocating fast-scanning probe has been designed to inject gas locally in the SOL for a duration of 8-10 ms, corresponding to a SOL width of ~ 5 mm. The system is capable of injecting up to 10^{19} molecules over the puff duration. Two near-perpendicular views of the probe are available, imaging impurity dispersal plumes using fiber optic bundles coupled to gated, intensified CCD cameras. Parallel and perpendicular impurity transport may be inferred from the dimension and structure of the plumes. Deep injections (i.e. at locations up to the separatrix) are achieved, allowing transport to be studied as a function of SOL position.

Initial plume experiments have been conducted using ethylene, with $\sim 5 \times 10^{16}$ molecules of gas typically injected per probe scan. Emission data has been aligned to machine coordinates, and absolutely calibrated. Plume extents parallel to the magnetic field are consistent with the calculation of ionization mean-free paths made using probe measurements. Radial electric fields inferred from cross-field dispersal of the impurities are also consistent with probe measurements. Cross-field flows are inferred from emission asymmetries, but a 3-D reconstruction of the emission is required to differentiate between flows in the flux surface (e.g. $\mathbf{E} \times \mathbf{B}$ flows) and flows across flux surfaces. Cross-field diffusion is inferred from differences in CII and CIII cross-field spreading. However, these differences are small, requiring accurate measurement of CII and CIII profiles, necessitating data for both charge states be collected from the same discharge.

In order to complete the diagnostic system, additional work is required. Future plans include: (1) Installation of a beam-splitter on both camera systems, allowing C^{+1} and C^{+2} data to be collected *simultaneously* from each view. Profile comparisons can then be used in 1-D modeling to infer D_{\perp} . (2) Application of a “slice” inversion algorithm to obtain projections in the R-Z plane of emission from a *limited* region of the plume. The full 3-D emission profile can

then be built up from various slices of emission. A non-negative least-squares algorithm [6] will be used to ensure the inverted emissivity $\varepsilon \geq 0$. (3) Monte Carlo modeling [7] to simulate the plume experiments, yielding parallel and perpendicular flows and diffusivities. The use of CII and CIII data obtained simultaneously will enforce tight constraints on the modeling, since the simulations will be required to reproduce results for both charge states.

Acknowledgements

This work is supported by US Department of Energy Contract No. DE-AC02-78-ET-51013.

References

- [1] D. Jablonski, B. LaBombard, G.M. McCracken, et al., J. Nucl. Mater. 241-243 (1997) 782.
- [2] B. LaBombard, S. Gangadhara, et al., J. Nucl. Mater. 266-269 (1999) 571.
- [3] Manufactured by Xybion Electronic Systems, Inc., 8389 Miralani Dr., San Diego, CA 92126.
- [4] B. LaBombard, private communication.
- [5] L.L. Lao, et al., Nucl. Fusion 25 (1985) 1611.
- [6] C.L. Lawson, R.J. Hanson, Solving Least Squares Problems, Prentice-Hall, Inc., 1974.
- [7] P.C. Stangeby, et al., Nucl. Fusion 28 (1988) 1945.